UWB pulse propagation into human tissues

OPEN ACCESS
IOP PUBLISHING PHYSICS IN MEDICINE AND BIOLOGY
Phys. Med. Biol. **58** (2013) 8689–8707 doi:10.1088/0031-9155/58/24/8689

UWB pulse propagation into human tissues

Marta Cavagnaro, Erika Pittella and Stefano Pisa

Department of Information Engineering, Electronics and Telecommunications, Sapienza University, Rome, Italy

E-mail: cavagnaro@diet.uniroma1.it

Received 8 May 2013, in final form 8 October 2013
Published 22 November 2013
Online at stacks.iop.org/PMB/58/8689

Abstract

In this paper the propagation of a UWB pulse into a layered model of the human body is studied to characterize absorption and reflection of the UWB signal due to the different body tissues. Several time behaviours for the incident UWB pulse are considered and compared with reference to the feasibility of breath and heartbeat activity monitoring. Results show that if the UWB source is placed far from the human body, the reflection coming from the interface between air and skin can be used to detect the respiratory activity. On the contrary, if the UWB source is placed close to the human body, a small reflection due to the interface between the posterior lung wall and the bone, which is well distanced in time from the reflections due to the first layers of the body model, can be used to detect lung and heart changes associated with the cardio-respiratory activity.

(Some figures may appear in colour only in the online journal)

1. Introduction

Ultra Wide Band (UWB) radars for remote sensing of vital signs, as the breath and the cardiac activity, are based on the detection of UWB pulses once reflected by the human body. The amplitude and phase variations as well as the time of arrival of the reflected pulse are used to evaluate the thorax and heart movements, to then derive the cardio-respiratory activities (Pisa *et al* 2012a).

Contrary to continuous wave (CW) radars, which transmit a CW signal at a specific frequency and detect frequency and phase changes due to the reflections from the target (Xiao *et al* 2006, Kim *et al* 2007, Pieraccini *et al* 2008, Varanini *et al* 2008, D'Urso *et al* 2009, Bakhtiari *et al* 2012, Sprager and Zazula 2012), UWB radars transmit a sequence of very short pulses whose frequency occupation is in the microwave range (typically from 3 to 10 GHz). Positive aspects of UWB radars are the low spectral density of the power associated with

the UWB pulses, the low sensibility to interfering signals, the capability of detecting objects close to the radar system, the high resolution, and the low-cost (Azevedo and McEwan 1996, Immoreev *et al* 2005).

The first UWB radar for remote sensing was patented in 1994 by McEwan at the Lawrence Livermore National Laboratory (LLNL) (McEwan 1994). Since then, several radar systems have been proposed, and studies have been conducted comparing the signals measured by UWB radars with those obtained from more traditional sensing techniques (Taylor and McEwan 2001, Staderini 2002, Bilich 2006, Pisa *et al* 2012b).

UWB radars for remote sensing are constituted by a pulse generator, a UWB receiver, a timing circuitry, a signal processor, and UWB antennas. The pulse generator is based on a pulse repetition interval generator with a repetition rate in the range 1–10 MHz, followed by a step-like generator producing a fast rise-time edge. Then, one or more impulse-shaping networks convert the fast edge in a signal whose time dependence is Gaussian like or a higher derivative of the Gaussian pulse (Andrews 2003). Subsequently, the signal is sent to the transmitting UWB antenna and it is radiated toward the target. Once reflected by the target, the impulse is received by a UWB antenna, detected by a suitable receiving section (Taylor and McEwan 2001, Dederer *et al* 2007) and processed to evaluate the distance between the antenna and the considered target.

Due to the particular applications of UWB radar in medicine, a fundamental point to investigate is the propagation of UWB pulses in human tissues both with reference to safety issues and in order to determine the optimum signal to monitor the cardio-respiratory activity.

Safety issues related to UWB radar have been considered in Cavagnaro *et al* (2013). Here it has been shown that if the transmitted signal fills the FCC emission mask defined as maximum Effective Isotropically Radiated Power (EIRP) measured on a specified bandwidth (FCC 02-48 2002), the limits settled to protect humans from possible adverse health effects of electromagnetic fields are fulfilled (ICNIRP 1998, 2009).

In this paper the propagation of UWB pulses in the human tissues will be studied. In particular, attention will be posed both on the tissue interfaces responsible for the signal reflection and on the definition of the best time behaviour of the incident pulse to be used to monitor the cardio-respiratory activity. To this end, pulses with time behaviour given by different derivatives of the Gaussian pulse will be taken into account. Moreover, both a fixed radar system, hypothetically placed on the room wall at a distance of 1 m from the patient to be monitored, and a wearable system, placed in a breast pocket, will be considered.

In order to better evidence the electric and geometric parameters influencing the UWB pulse propagation into the human tissues, the study is conducted considering a multilayer planar model of the human body. Multilayer planar models have been already used to predict UWB signal attenuation into different layers from the skin to the heart and back (Staderini 2002, Varotto and Staderini 2011). In Staderini (2002) the multilayer model was derived from the Visible Human (VH) data set (Ackerman 1998), and the dielectric properties of the considered tissues were not dependent on the frequency, while in Varotto and Staderini (2011) the dependence of the dielectric properties from the frequency was included in the model. In both papers, the attenuation was evaluated without including multiple reflections at the several interfaces comprising the model, and the obtained results were presented as a function of the frequency. In this paper, a more standard anatomical body model will be used to derive the multilayer planar model, and the dispersive behaviour of the electromagnetic properties of the human tissues will be considered. To validate the considered model the signal attenuation as a function of the frequency will be evaluated and compared with the previously obtained results (Varotto and Staderini 2011). Then, the signal propagation and reflection will be simulated in the time domain, including multiple reflections from the different layers, to

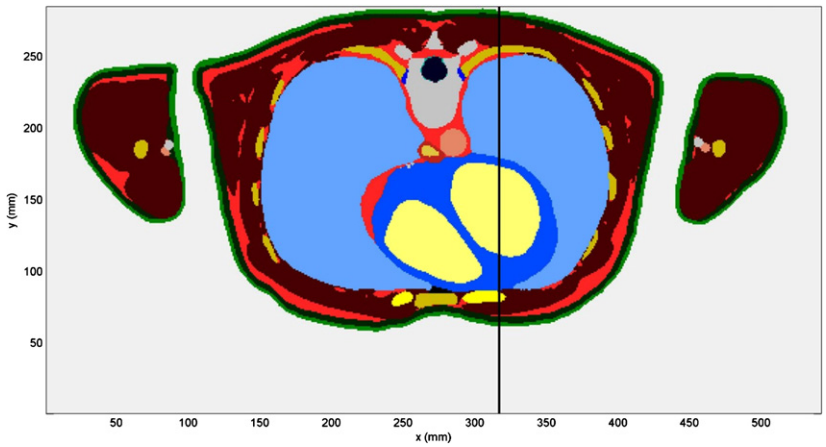

Figure 1. Axial section of the Duke's anatomy used to construct the multilayer planar model. The line considered to obtain the layers' sequence is evidenced.

put into evidence specific signal behaviours. The study will be conducted through simulations performed with both a circuital and a full-wave electromagnetic software package.

2. Methods and models

2.1. Multilayer body model

Simple models of the human anatomy are useful to evidence the main mechanisms underlying electromagnetic field interaction with the human tissues. With reference to UWB signal propagation, a multilayer planar model of the human thorax, derived from the VH data set, was used by Staderini (2002) to predict signal reflection and attenuation into the different layers. However, the so-called 'Virtual population' has been recently developed, comprising a man (Duke, 34 years old), a woman (Ella 26 years old), and several children (Christ *et al* 2010). While the VH model represents a relatively 'big man' (1.80 m tall, 103.0 kg weight), Duke, being 1.77 m tall, and weighting 72.4 kg, is closer to the 'standard man' dimensions (ICRP 1975, Ellis 1990). To build the multilayer planar model, a section of the Duke's anatomy passing through the heart has been considered. Figure 1 shows the considered section as well as the line used to obtain the layers' sequence for the planar model. The multilayer planar model is depicted in figure 2.

2.2. Numerical methods

Simulations have been performed considering the absorption and reflection of a plane wave, with a UWB frequency spectrum, impinging orthogonally (y-axis in figure 2) on the surface of the planar multilayer model. The reflection coefficient at the air–skin interface, the transmission into the layers, the reflections at the interfaces between the different layers, and the time behaviour of the pulse propagating into the different tissues can be evaluated by using the transmission line formalism, which substitutes to each tissue layer a transmission line of the same length. Each transmission line is characterized by its propagation constant and characteristic impedance both dependent on the frequency and on the dielectric properties of the corresponding tissue. Since the considered signals have a UWB frequency occupation,

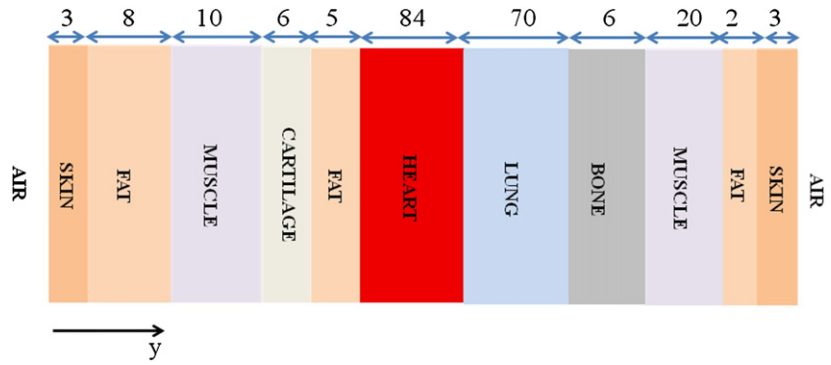

Figure 2. Multilayer planar model derived from the Duke's anatomy (the data above the layers report layer thicknesses in mm—the layers are not in scale).

the dispersive behaviour of human tissues has been taken into account through the Cole–Cole model (Cole and Cole 1941) using the parameters computed in Gabriel *et al* (1996b).

The time and frequency behaviours of the incident and reflected signals reported in the following sections have been computed with the circuital CAD MWO^{TM} (AWR El Segundo, CA) by using the harmonic balance solver.

To validate the results obtained with MWO, the full-wave electromagnetic solver Microwave Studio^{TM} (MWS–CST Darmstadt Germany) has been used. In MWS, the plane wave propagating into the multilayer planar model has been simulated through a parallel plate transmission line, filled with the dielectric layers of figure 2. However, since in MWS the dielectric dispersion is represented according to the Debye's model (Debye 1929), the comparison between MWS and MWO has been conducted considering a first order Debye dispersion mechanism for the dielectric properties of tissues. Moreover, a plane wave propagating into a vertical section (7 cm high) of the Duke's thorax has been also studied to put into evidence the representativeness of the multilayer model. When an anatomical model of the human body is studied, as in this case, MWS does not allow us to introduce the dielectric properties' dependence on the frequency; so, the values at 2 GHz have been used (Gabriel *et al* 1996b, accessible online at http://niremf.ifac.cnr.it/tissprop/htmlclie/htmlclie.htm).

Finally, to deepen the validity of the obtained results, Monte Carlo simulations have been performed in MWO randomly changing both the dielectric properties of the considered tissues and the thicknesses of the tissues' layers. A maximum deviation of $\pm 10\%$ from the nominal values has been allowed, according to the spread on the measured values reported in Gabriel *et al* (1996a).

2.3. UWB pulses' amplitude definition with reference to FCC mask compliance

In order to evaluate the feasibility of breath and heartbeat activity monitoring through UWB radar, it is fundamental to correctly define the amplitude of the signal impinging on the human body. Since UWB radar emissions should be compliant with compatibility emission masks issued by regulatory bodies, these masks have been used to evaluate the maximum amplitude allowed for the UWB pulses.

In USA, the Federal Communications Commission (FCC) issued regulations for UWB medical imaging systems allocating a frequency band between 3.1 and 10.6 GHz and defining the EIRP measured on a specified bandwidth (FCC 02-48 2002). In Europe, the European Technical Standard Institute (ETSI) in close cooperation with the Electronic Communications

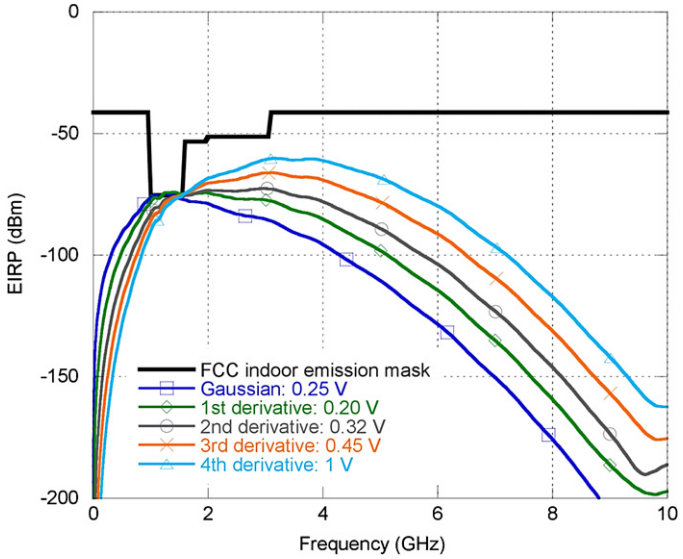

Figure 3. Computed EIRP for various time behaviours of UWB pulses. The maximum amplitude that gives rise to EIRP in compliance with FCC indoor emission mask is reported for each pulse.

Committee (ECC) developed a regulation, approved by the European Commission in 2009, with limits for the maximum EIRP allowed for UWB indoor communications (EC 2009).

Since in this work a medical application is considered, the shape and amplitude of the UWB pulses have been made compliant with the FCC emission mask. Being this mask defined in terms of EIRP, which includes both the radiated power and the directivity of the antenna, to evaluate the maximum amplitude of the source signal the pulse radiated by a half-heart shaped antenna (Pittella *et al* 2011), fed by a sequence of UWB pulses with a repetition rate of 1 MHz and various time behaviours, has been considered. In particular, the Gaussian pulse with standard deviation (σ) of 100 ps and its first four derivatives have been studied (Cavagnaro *et al* 2013). For each pulse, the maximum source amplitude that gives rise to an EIRP in compliance with the FCC emission mask has been computed as reported in figure 3.

Figure 3 shows that the peak in the spectrum of the pulses with time behaviour given by higher derivatives of the Gaussian pulse shifts toward higher frequencies. Accordingly, being their frequency spectrum better centred with respect to the FCC emission mask, higher amplitude values can be considered for the source voltage. To translate the obtained source's amplitudes into electric field values, two different approaches have been used for the fixed and the wearable radar systems, respectively.

In the case of fixed radar system, where a distance between the radar and the subject of about 1 m is considered, the same MWO model employed to evaluate the EIRP has been used to evaluate the corresponding electric field, by way of an electric field probe in the time domain. Starting from the first derivative of the Gaussian pulse with a source amplitude of 0.2 V, a maximum electric field value of 0.111 V m^{-1} has been thus obtained. The amplitudes of 0.149, 0.308, 0.578 V m^{-1} have been obtained for the second, third and fourth derivatives of the Gaussian pulse, respectively.

In the case of wearable radar system, where a distance between the radar and the subject of about 1 cm is considered, the body model is in the near field of the radiating antenna. In this case, to obtain the maximum electric field value which corresponds to the source amplitudes compliant with the FCC mask, an electromagnetic simulation has been performed with MWS.

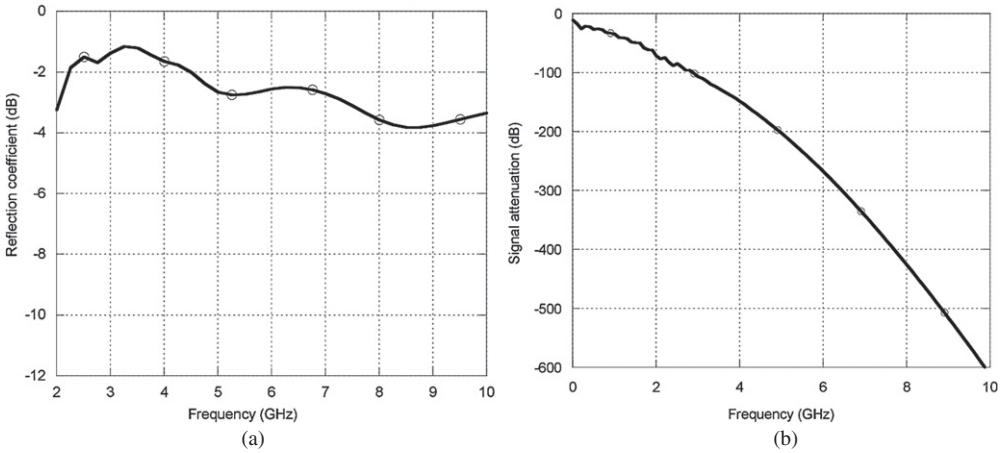

Figure 4. (a) Reflection coefficient of a plane wave impinging on the Duke planar model and (b) signal attenuation considering the propagation from the air to the lung and back.

In particular, the previously cited half-heart shaped antenna (Pittella *et al* 2011) has been considered in front of an indefinite homogeneous slab with the properties of 2/3 muscle, and it has been excited with a monocycle pulse with a maximum amplitude of 0.2 V. Then, the time behaviour of the electric field inside the box has been recorded, obtaining a maximum amplitude equal to 10.5 V m^{-1}.

In the following, the obtained values will be used as the maximum amplitudes of the incident plane wave to study the propagation of the different pulses in the multilayer planar model.

3. UWB pulse propagation into the multilayer thorax model

3.1. Signal attenuation and reflection

Figure 4(a) shows the reflection coefficient of a plane wave impinging orthogonally on the multilayer model as a function of the frequency, while figure 4(b) shows the attenuation undergone by a plane wave travelling into the multilayer model (*y* axis of figure 2), from the skin layer to the lung and the way back, as a function of the frequency.

From figure 4(a) it can be noted that the reflection coefficient is approximately equal to −3 dB in the whole considered frequency band, that means that about half of the electromagnetic power incident on the multilayer model is reflected back and half is transmitted into the body. From figure 4(b) it can be noted that the attenuation of the signal is close to −100 dB at 3 GHz and that it increases dramatically with the frequency. These data are in agreement with those obtained in Varotto and Staderini (2011) where a signal attenuation of −93 dB has been evaluated at 3.1 GHz for a different body model.

3.2. Time behaviours of UWB pulses with reference to the interaction with the multilayer body model

The UWB incident pulses as well as the pulses reflected back from the multilayer body model are shown in figure 5 considering a distance between the UWB source and the body model equal to 1 m. In figures 5(a)–(d) the incident signals have a time behaviour equal to the first four derivatives of the Gaussian pulse, and the maximum amplitude allowed by the FCC mask,

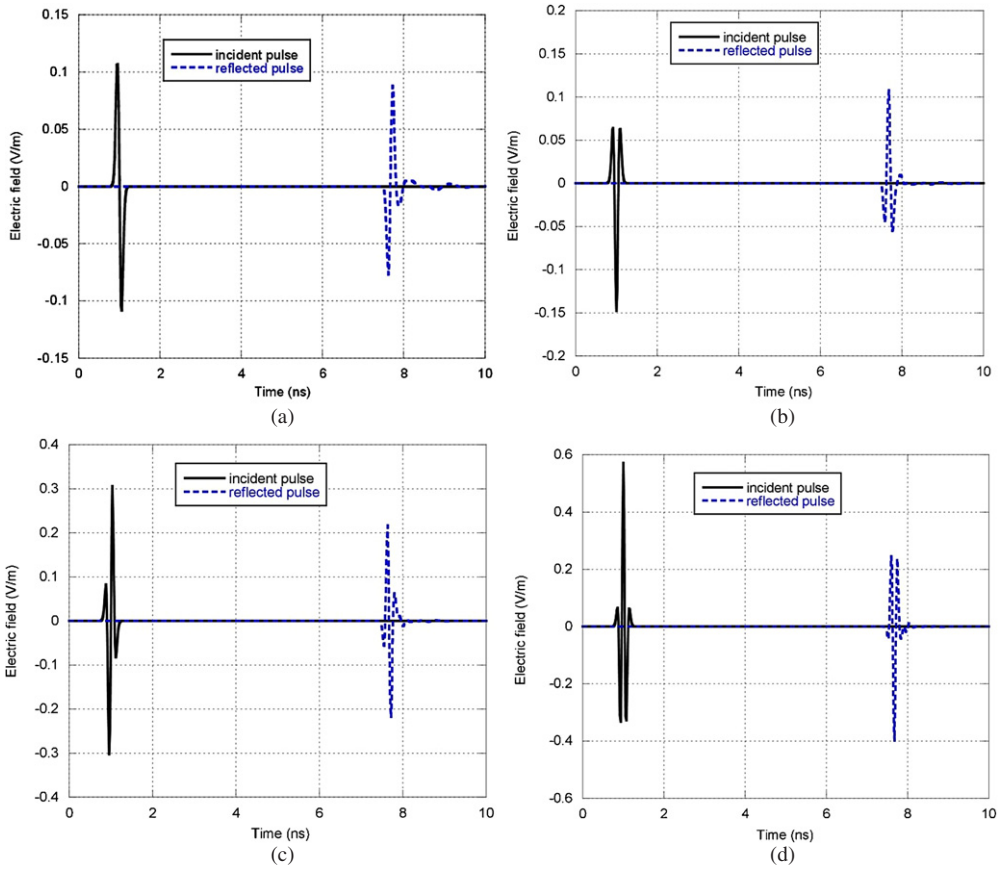

Figure 5. Time behaviour of the pulse incident on and reflected by the multilayer body model when the first (a), second (b), third (c) and fourth (d) derivatives of the Gaussian pulse are considered. The amplitudes of the incident signals are those reported in section 2.3.

as obtained in section 2.3. From figure 5 it can be noted that the first reflected signal, due to the interface between air and skin, arrives at the location of the UWB antenna after about 7 ns from the onset of the incident signal, corresponding to a round trip 2 m long. Moreover, the reflected pulses show an inversion with respect to the incident ones caused by a negative value of the reflection coefficient, which in turn is due to the lower value of the impedance of the human body with respect to the free space impedance.

To look at the reflected signals with higher detail, figure 6 shows a zoom of the four reflected signals between 5 and 20 ns. From figure 6 it can be noted the presence of a small reflected pulse coming later in time after the initial reflections. In particular, it is interesting to note that this small signal appears at exactly the same time for all the considered cases, i.e. after about 9 ns from the onset of the first reflected signal.

Considering an average dielectric constant of 50 for the different tissues comprising the thorax model at the different frequencies considered, the speed of the electromagnetic field into the biological tissue is

$$\frac{3 \cdot 10^8}{\sqrt{50}} \quad \mathrm{m\,s^{-1}} \approx 0.42 \cdot 10^8 \ \mathrm{m\,s^{-1}},$$

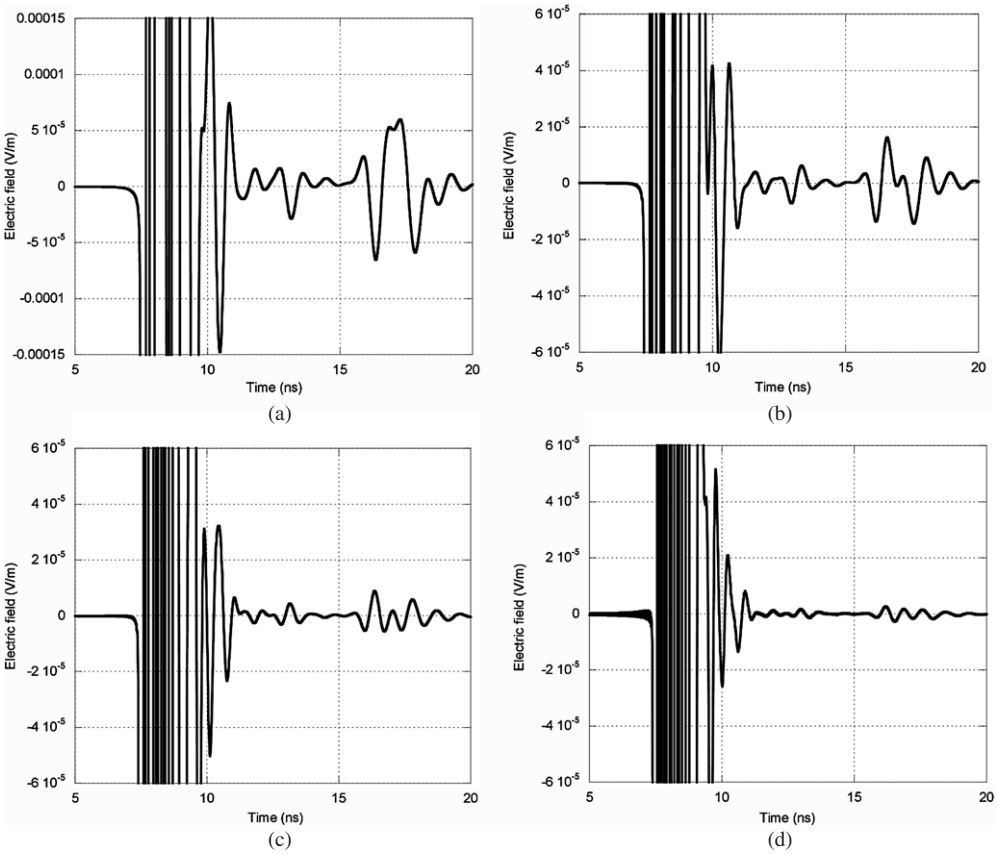

Figure 6. Zoom in of the time behaviour of the reflected pulse, when the first (a), second (b), third (c) and fourth (d) derivatives of the Gaussian pulse are considered. The amplitudes of the incident signals are those reported in section 2.3.

and the distance covered in 9 ns is

$$d = 0.42 \cdot 10^8 \times 9 \cdot 10^{-9} = 37.8 \text{ cm}.$$

Accordingly, it could be argued that the reflection comes from a layer located about 19 cm deep into the model. At this distance the interface between the lung and bone is found (figure 2). To explain why the interface between lung and bone should be different from the other interfaces, it can be noted here that the lung dielectric properties used in the simulations are those of deflated lung, which show a high discontinuity with the bone characteristics, as shown in figure 7 where the permittivity of the different tissues comprising the multilayer model are reported at 3.0 and 10.0 GHz. Figure 7 evidences that, at 3 GHz, the relative dielectric constant of deflated lung is equal to 48, while that of bone is 12; similarly, at 10 GHz, deflated lung shows a relative dielectric property of 40, while bone presents a value of 9. From figure 7 a great discontinuity can be observed between fat and heart also, and at the interface between bone and muscle. However, the interface between fat and heart is located at 3.2 cm from the surface of the model (see figure 2), so that the signal reflected by this interface covers the round trip from the skin to the heart and back in about 1.5 ns, and arrives nearly superimposed to the air–skin reflection.

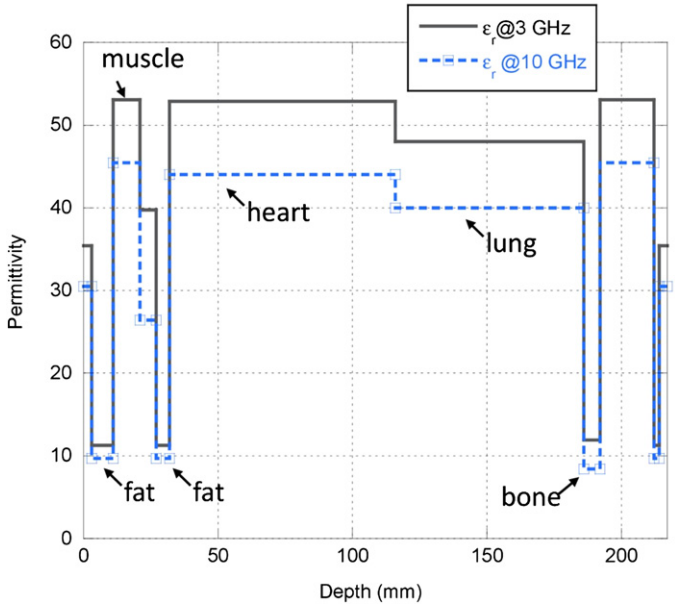

Figure 7. Relative dielectric constant of the tissues in the thorax model at 3.0 and 10 GHz as a function of the position within the model.

To discriminate among the other possible reflections, and to verify that the small reflected signal found at about 16 ns effectively comes from the lung–bone interface, further simulations have been carried out. To this end, the geometry of the multilayer model has been changed considering the lung with an indefinite length, or considering the bone with an indefinite length. In the first case, lung with an indefinite length, the pulse reflection at 16 ns was not present any more in the reflected signal; in the latter case, bone with an indefinite length, the reflection was still there, even if with a slightly different time behaviour with respect to that depicted in figure 6. Moreover, a model with the layer of muscle behind the bone with an indefinite length was studied also, finding that the reflection was still evident with very small changes in its time behaviour. Since the indefinite length of a layer gives a matching condition, i.e. no reflections are obtained at the end of the layer, the obtained results show that the pulse reflection at 16 ns is obtained from the lung–bone interface.

Concerning the amplitude of the reflected pulses, figure 5 shows that the pulses reflected by the air–skin interface have more or less a −3 dB reduction with respect to the incident pulses (the maximum amplitude of the reflected signal is about 0.707 of that of the incident one), in agreement with figure 4(a).

On the contrary, figure 6 shows that even if the incident pulses have amplitudes higher for higher derivatives of the Gaussian pulse, the pulses reflected by the lung–bone interface have lower amplitudes for higher derivatives. This result can be understood considering that, according to figure 3 and thanks to the frequency behaviour of the FCC mask, higher amplitudes can be used for the source signal when higher derivatives of the Gaussian pulse are used; on the other side, these signals, having a higher frequency content, undergo a higher attenuation while travelling into the different tissues, as obtainable from figure 4(b). In this respect, it is interesting to note from figures 5(a) and 6(a) that the signal reflected by the lung–bone interface shows an attenuation of approximately −60 dB from the incident signal. If the attenuation undergone by a plane wave travelling from the skin layer to the bone and the

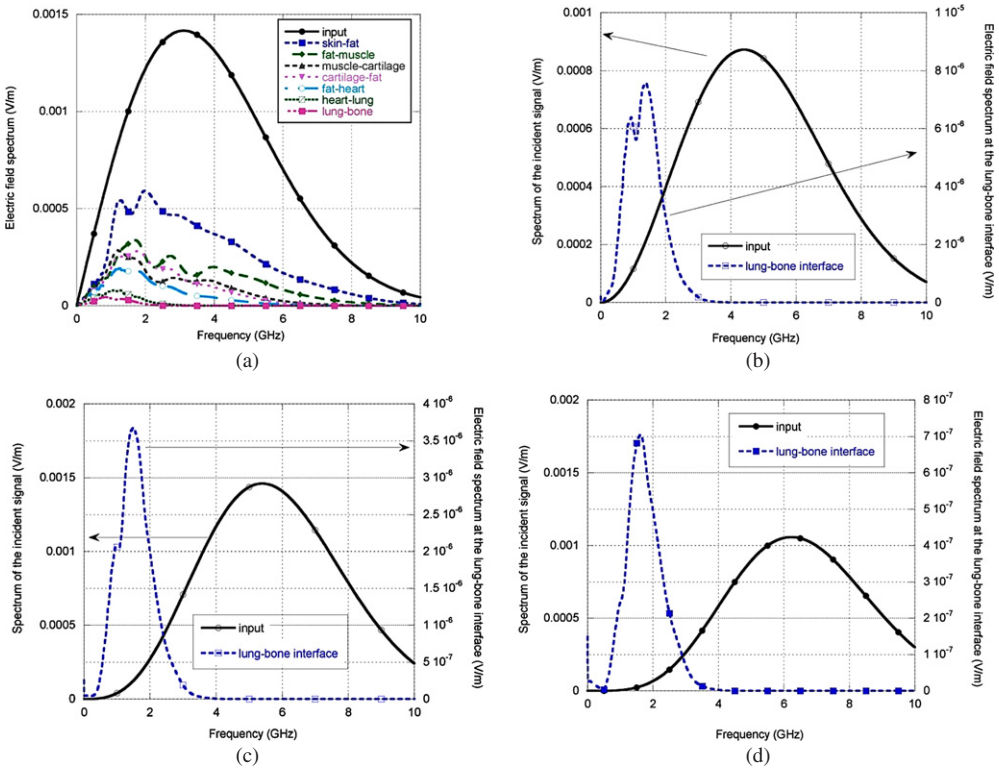

Figure 8. Spectrum of the incident pulses and of the pulses arriving at the lung–bone interface, when the incident pulse is given by the (a) first, (b) second, (c) third and (d) fourth derivative of the Gaussian pulse. (a) reports the spectrum of the pulse at the different interfaces of the multilayered model, also.

way back is evaluated as a function of the frequency, the value of −60 dB is obtained at about 2 GHz. Accordingly, it can be argued that the pulse reflected back from the innermost layers is composed by the lower frequencies, which are those that undergo a lower attenuation while travelling into the different body tissues. To confirm this hypothesis, figure 8 shows the spectrum of the signal travelling into the different body layers compared with the spectrum of the incident signal, for the four time behaviours considered (figures 8(a)–(d)).

From the figure it can be noted the different frequency occupation of the incident pulses, with the maximum value moving toward higher frequencies for higher derivatives of the Gaussian pulse (from figures 8(a)–(d)), as well as the frequency occupation of the pulses arriving at the lung–bone interface. In particular, it is interesting to note from figure 8(a), where the spectra of the signal are reported at the different interfaces present into the multilayer model, how the spectrum of the signal changes while travelling into the body, losing the higher frequencies. At the lung–bone interface the frequency occupation of the four signals is very close to each other.

As a validation of the results obtained with the circuital solver MWO, a simulation has been performed with the full electromagnetic solver MWS. As stated in section 2.2, since in MWS the frequency dependence of the dielectric properties is defined according to the Debye's model, the same dispersion model has been used in MWO in this test case. Figure 9 shows the reflected pulses evaluated by the two software packages when the monocycle impinges on the multilayer planar model.

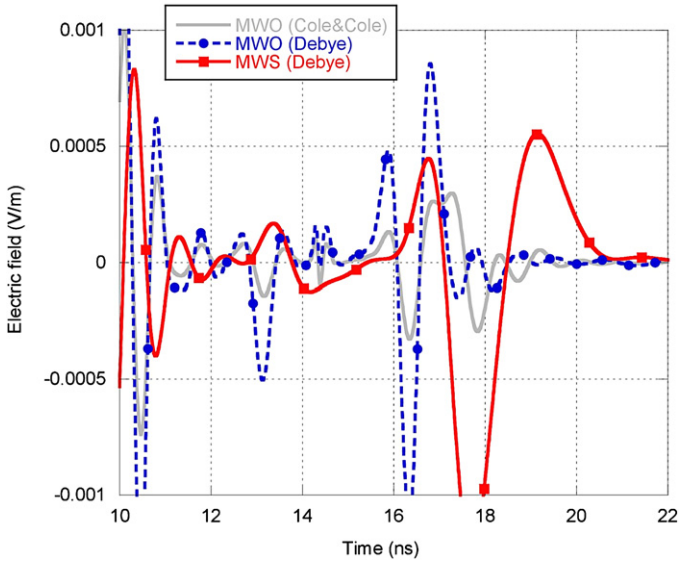

Figure 9. Reflected pulse obtained by MWS and MWO when the first derivative of the Gaussian pulse is considered.

From the figure good agreement between the two results can be obtained both with reference to the amplitude of the reflected signal and to its time of arrival. From figure 9 it is interesting to note that the model used to represent the dispersion of tissues' dielectric properties influences the obtained results. In particular, the Debye's model leads to higher signal amplitudes than those obtained with the Cole–Cole model.

4. Monitoring of vital signs with a fixed UWB radar system

In this section the performances of a fixed radar system have been investigated, considering the radar placed on a wall of a room. The distance between the source/receiver and the thorax model has been taken equal to 1 m. This situation could be representative of the continuous monitoring of patients in intensive care, i.e. confined in bed all day long.

The study is conducted considering as incident signal a plane wave with time behaviour given by the monocycle pulse (first derivative of the Gaussian pulse) due to the higher amplitude obtained for the late-in-time reflected signal with respect to the other time behaviours considered. Starting from the multilayer model reported in figure 2, which represents a resting condition with the lung deflated, two different models of the respiratory activity will be studied: in the first case the lung dimension will be increased to simulate the inspiration phase (extended lung); in the second model, the lung dimension will be increased and the lung dielectric properties will be changed to represent the tissue made of air and lung cells (inflated lung).

4.1. Breath activity monitoring

To simulate the breath activity increasing lengths for the layer representing the lung have been considered, according to the inspiration and expiration of the air; a corresponding reduction of the distance between the radar antenna and the body has been then introduced. In particular, the lung length was 70 mm in the initial thorax model (figure 2), corresponding to a resting

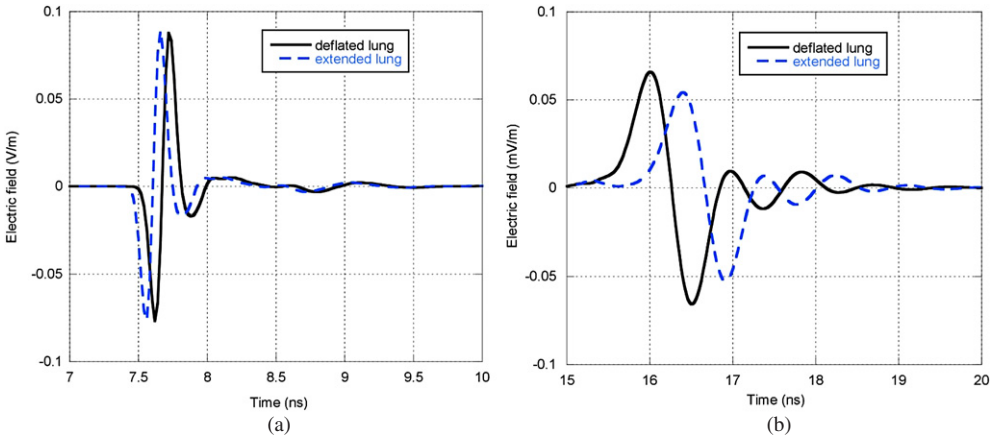

Figure 10. Time behaviour of the reflected pulse arriving at the receiver location in the case of lung deflated and lung extended. (a) Time window between 7 and 10 ns; (b) time window between 15 and 20 ns.

state with a deflated lung. This length has been increased up to 80 mm (extended lung), corresponding to a tidal breath.

The resting state is close to the situation studied in the previous section. Accordingly, the reflection coming from the skin layer will arrive after about 7 ns from the centre of the incident pulse, while the signal reflected by the lung–bone interface will arrive about 9 ns after the pulse coming from the skin. Since the source is centred in time at 1 ns, the first reflection will arrive at about 8 ns, and the reflection from the bone at about 17 ns. Figure 10(a) shows the reflected signals arriving at the receiver location obtained from the two planar models with deflated lung and extended lung in the time window from 7 to 10 ns, while figure 10(b) shows the same signals from 15 to 20 ns.

As it can be noted from figure 10, the two cases of deflated lung (resting phase) and extended lung are clearly discernible in time. Indeed, the peak of the reflected pulse coming from the skin is at 7.72 ns in the case of resting state and at 7.66 ns in the case of extended lung (figure 10(a)), corresponding to a movement of 9 mm. A similar time shift can be obtained from the later reflected pulses. Looking at the vertical scales of figure 10, it is evident that, when the radar system is placed far from the body, the respiratory activity can be monitored looking at the signal reflected by the air–skin interface.

As stated before, the dielectric properties of deflated lung are different from those of bone. However, during the inspiration phase, the lung extends due to air inhalation. Accordingly, the dielectric properties of lung change together with lung dimensions, lowering with respect to the values of deflated lung. As an example, the relative permittivity of inflated lung is 20.13 at 3 GHz, and 16.15 at 10 GHz (Gabriel 1996b, accessible online at http://niremf.ifac.cnr.it/tissprop/htmlclie/htmlclie.htm).

To investigate if the different dielectric properties influence the signal reflection, figure 11 shows the time behaviours of the reflected signals arriving at the receiver location in the case of resting state (deflated lung) and in the case of tidal breath, modelled with a lung extension of 80 mm and using the dielectric properties of inflated lung (inflated lung).

Comparing figures 10 and 11, it can be noted that while no difference is obtained in the signal reflected by the air–skin interface when extended or inflated lung is considered (figures 10(a) and 11(a)), a different behaviour between the signals reflected in the two lung models is evident in the late-in-time reflection (figures 10(b) and 11(b)). In particular, the

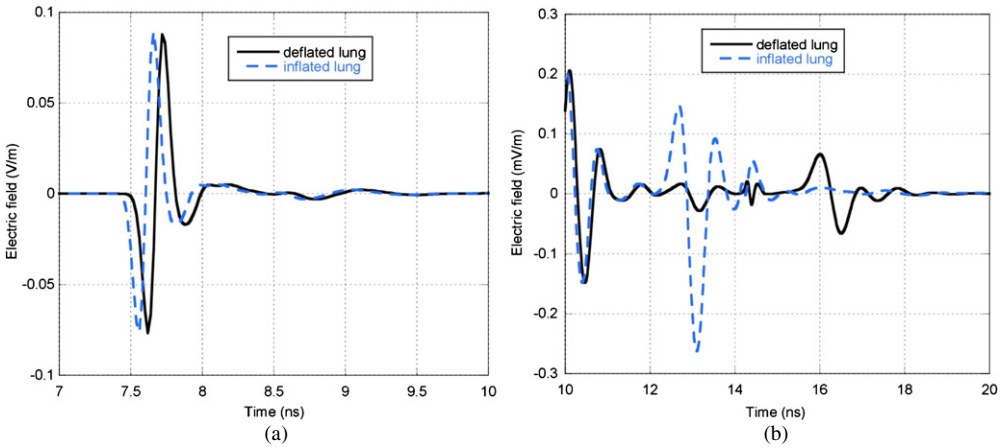

Figure 11. Time behaviour of the reflected pulses at the receiver location in the case of deflated lung (resting state) and lung inflated (tidal breath). (a) Time window between 7 and 10 ns; (b) time window between 15 and 20 ns.

reflection from the inflated lung comes earlier and with greater amplitude than the reflection from the extended lung. Accordingly it can be derived that in this case the late reflection does not come from the lung–bone interface anymore, but from the heart–lung interface that, when the lung is inflated, represents an interface between two tissues with significant differences in the dielectric properties, more than the interface between inflated lung and bone.

5. Monitoring of vital signs with a wearable UWB radar system

In this section the functioning of a wearable radar system has been investigated, considering the radar placed in a breast pocket to monitor the respiratory and cardiac activity during a normal living day. As in the preceding section, the study is conducted considering a plane wave with time behaviour given by the monocycle pulse as incident signal.

5.1. Breath activity monitoring

If the radar is placed on the thorax (skin–radar distance of about 1 cm), the signal reflected back from the skin will not be discernible from the incident signal due to the very short time needed to cover the distance between the transmitting antenna and the thorax and the way back. Moreover, since the skin layer will move together with the radar device, the first reflection from the thorax will have no differences between resting and tidal phases. However, as described in section 3.2, the reflection coming from the lung–bone interface could allow detecting the breath activity.

Figure 12(a) shows the reflected signals in the two cases of deflated lung (resting state) and extended lung, while figure 12(b) shows the reflected signals in the case of deflated lung and tidal breath, this latter case simulated with the dielectric properties of inflated lung together with a higher dimension of the lung. From figure 12 it can be noted that the different lung length changes the time of arrival of the pulse reflected from the lung–bone interface, and that modifying both the lung length and lung dielectric properties a change both in the amplitude and in the time of arrival of the reflected signal is obtained (figure 12(b)). This last result is the same obtained in the case of a fixed radar system, and it can be explained accordingly, i.e.

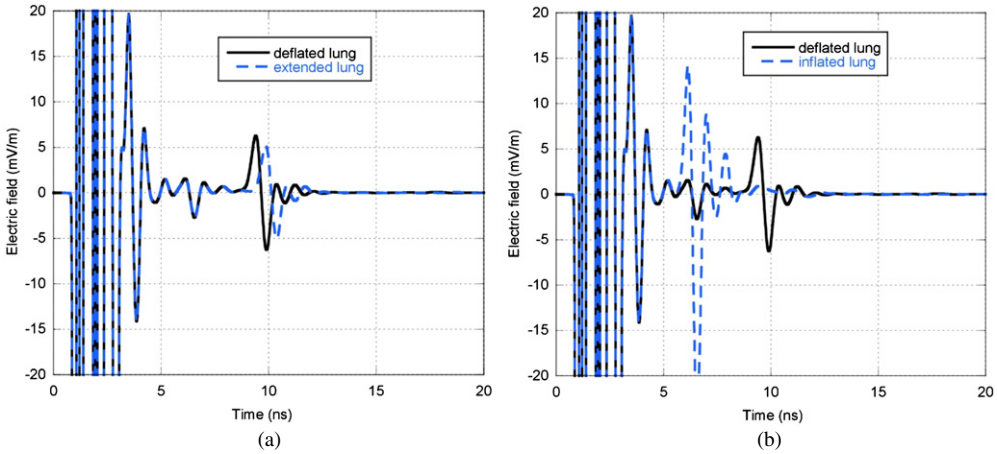

Figure 12. Time behaviour of the reflected pulse from the bone–muscle interface. (a) Deflated lung and lung extended; (b) deflated lung and tidal breath.

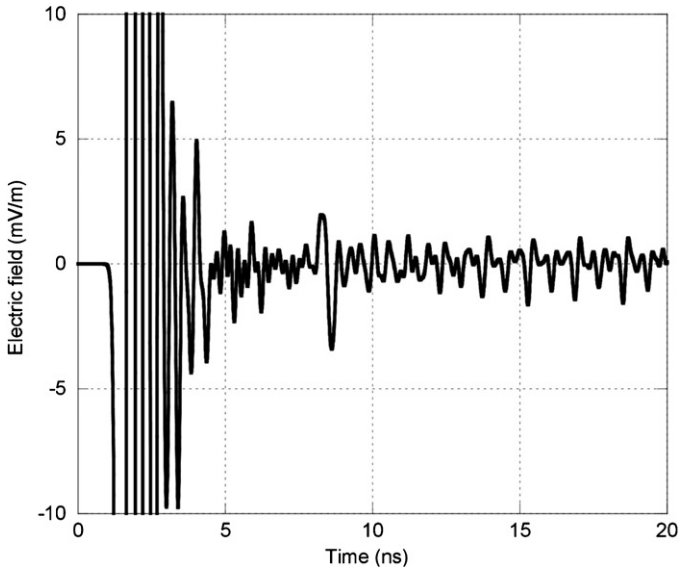

Figure 13. Time behaviour of the reflected pulse in the case of deflated lung obtained by an anatomical vertical section of the Duke's model by MWS.

the reflection of the UWB pulse is obtained in this case at the interface between the heart and the inflated lung.

To find out differences between the obtained results and those achievable using an anatomical model, a full-wave electromagnetic simulation has been performed with MWS considering a plane wave incident on part of the Duke's thorax, at the height of the section depicted in figure 1. As detailed in the methods section, in this case the dielectric properties of the tissues have been taken equal to the values at 2.0 GHz.

Figure 13 shows the reflected pulse obtained by MWS. The late-in-time reflected pulse is clearly evident, even if more oscillations can be noted with respect to the pulse reflected by the multilayer planar model.

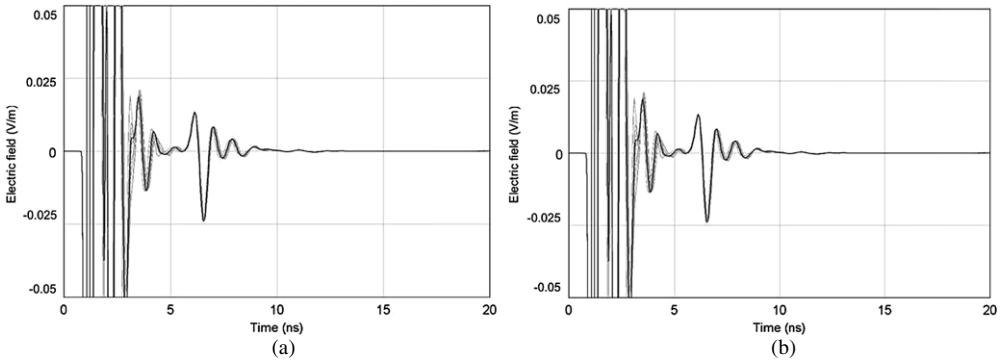

Figure 14. Monte Carlo results related to the time behaviour of the pulse reflected by the bone–muscle interface in the case of deflated lung. (a) 20 iterations allowing a $\pm 10\%$ change in both dielectric properties and thicknesses of all tissues' layers; (b) 20 iterations allowing a $\pm 10\%$ change in the dielectric properties of the skin only.

Finally, to deepen the validity of the obtained results, a Monte Carlo simulation has been conducted changing both the dielectric properties and the thicknesses of the considered tissues. In particular a maximum deviation of $\pm 10\%$ from the initial values has been allowed. Moreover, to put into evidence the influence of the skin layer, a Monte Carlo simulation has been performed changing only the skin properties. Figure 14 shows examples of the obtained results considering the reflected pulse in the case of inflated lung.

In particular, figure 14(a) reports 20 Monte Carlo iterations allowing a $\pm 10\%$ change in both thickness and dielectric properties of all the tissues making the multilayer model, while figure 14(b) shows the outputs obtained allowing a $\pm 10\%$ change of the dielectric properties of the skin only. From the figure it can be noted that small differences both in the amplitude and in the time of arrival are obtained in the reflected pulse, thus confirming the validity of the obtained results.

5.2. Cardiac activity monitoring

To model the cardiac activity, the lung has been considered in a resting state while the heart length has been changed from 74 to 94 mm with a 5 mm step.

Figure 15 shows the reflected signals in the time window from 6 to 12 ns for the five considered heart dimensions. The figure evidences that the different dimensions are clearly discernible from the time of arrival of the peak of the received UWB waveform.

6. Discussion

UWB radar applications are based on the detection of a target and its movements without the need of a direct contact between the radar and the target (Azevedo and McEwan 1996). The most recent applications are related to medical imaging, and in particular to the detection of the cardio-respiratory activity of a subject (Staderini 2002, Zito *et al* 2008, Serra *et al* 2010, Pisa *et al* 2012b). This can be used in intensive-care units, in pregnancy monitoring, for the measurement of the cardiac volume, and to prevent some syndromes of the respiratory apparatus, as the sudden-infant-death syndrome.

While several studies have been conducted to evaluate the feasibility of cardio-respiratory activity monitoring with UWB radars (Bilich 2006, Suzuki *et al* 2012, Zito *et al* 2008), and to develop the different circuital parts (e.g. Andrews 2003, Pisa *et al* 2012b, Pittella *et al* 2011,

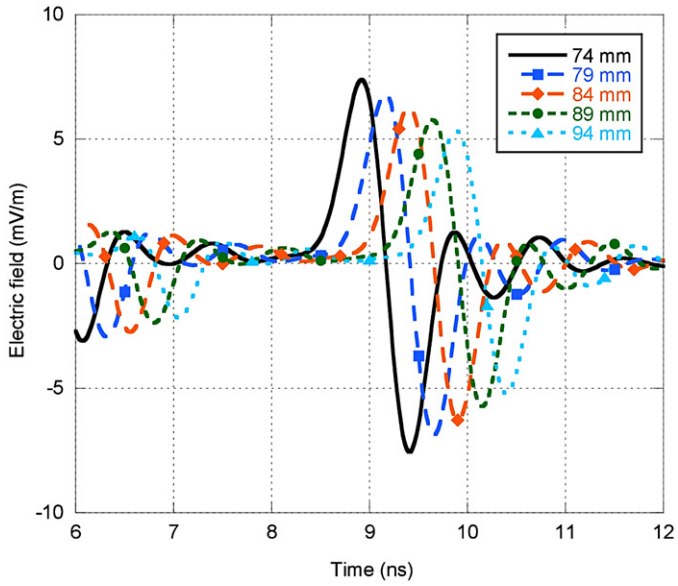

Figure 15. Time behaviour of the received pulse, when the thickness of the heart layer is changed from 74 to 94 mm.

Serra *et al* 2010), few studies have been conducted to characterize UWB signal propagation into the human body (Staderini 2002, Varotto and Staderini 2011, Cavagnaro *et al* 2013). Staderini (2002) used a multilayer body model to evaluate signal attenuation and time of propagation in the different tissues. A similar study was conducted in Varotto and Staderini (2011) where the very high attenuation obtained as a function of the frequency in the UWB band (3–10 GHz) was interpreted as the impossibility of obtaining a reflection from the inner body layers adequate to detect the heartbeat activity. A different mechanism was then proposed, linked to the antenna matching.

In this paper a numerical study has been conducted to evaluate the interaction between UWB pulses and the human body with the aim of evidencing the characteristics of signal propagation into the different tissues of the human body. To this end, a multilayer body model has been considered, starting from a section of the Duke's anatomy passing through the heart. Since the incident pulse has a UWB frequency occupation, the dispersive characteristics of the tissues' dielectric properties have been included in the model.

The incident signal has been modelled as a UWB pulse with several time behaviours and with the characteristics of a plane wave incident orthogonally on the model. The frequency and time behaviour of the reflected pulses have been evaluated through the circuital MWO software.

Looking at the reflected signals, it has been shown that the reflection from the air–skin interface can be used to detect thorax movements due to the respiratory activity when the radar is placed at distance from the human body. In this case, no differences have been obtained linked to the different time waveforms considered.

On the other side, when the radar is placed in contact with the human body, the reflection due to the air–skin interface cannot be used any more because it comes nearly superimposed to the incident signal and it does not change with the thorax movements since the radar changes its position together with the thorax. However, the obtained results show that, within the reflected pulse, after some time, a small oscillation is clearly detectable. Moreover, it has

been noted that this small oscillation is generated by the interface between the posterior wall of the lung and the bone, and that it changes when the lung changes its length and dielectric characteristics due to air inhalation. Accordingly, this small reflection can be used to detect the respiratory activity when a wearable radar is considered. Finally, it has been shown that the same small oscillation can be used to detect changes in the heart dimensions due to the cardiac activity, also. It can be noted here that, if a cardio-respiratory monitoring is required, the heartbeat signal can be easily distinguished from the breath one due to the different rates of the two considered activities. In fact, the breath activity shows a frequency of $f_B = 0.2$ Hz, while the cardiac activity of $f_H = 1.2$ Hz.

Comparing the different time behaviours of the incident signal, it has been shown that the small oscillation has more or less the same amplitude even if the incident signals have different amplitudes according to the FCC mask. To understand this point the different frequency occupation of the incident pulses must be considered: the higher the derivative of the Gaussian pulse used, the higher the frequency content of the pulse, and the higher the attenuation undergone by the pulse during its way into the human tissues (figure 2). In particular, due to the very high attenuation undergone by the field at high frequencies, the higher frequency components tend to be completely attenuated during their way into the tissues, according to Varotto and Staderini (2011), and the signal reflected by the inner structures of the body, detectable by the UWB receiving antenna, is mainly composed by the lower frequency content of the incident signals. This result is in close agreement with that obtained by Moten *et al* (1989) where the propagation of pulses into the human tissues was studied by way of the Fourier series to compare the depth of penetration of pulse trains with that of CW signals.

With reference to the amplitude of the reflected signal, UWB receivers are based on the range gating technique, which consists of receiving the reflected signals in a narrow time window. In particular, the receiving window is opened after each transmitted pulse with a delay time defined by the distance at which the object to be detected is located. In this way, interference from other signal sources is minimized. Moreover, thousands of received pulses are integrated before extracting the useful signal, in order to increase the signal to noise ratio (Azevedo and McEwan 1996, Immoreev *et al* 2005). Receiver sensitivities of about -77 dBm have been reported (Immoreev *et al* 2005). Considering a 50 Ω matched receiver and the link between voltage and electric field evaluated in section 2.3, a minimum receivable electric field of about 0.015 mV m^{-1} can be evaluated. Since it has been noted that the late-in-time reflected signal is about -60 dB below the incident one, i.e. in the case of the monocycle each reflected pulse has a level of about 0.05 mV m^{-1}, and considering the averaging done on the received pulses, it can be concluded that the reflected pulse amplitude is higher than the typical receiver sensitivities.

The presented results have been obtained considering a plane wave impinging on a multilayer model of the human body. While the plane wave approximation can be surely used when the fixed radar system is studied, in the case of a wearable system the human body is in the near field of the antenna. However, at 3 GHz, the wavelength into the tissue is about 1 cm (at 10 GHz it is about 3 mm), so that at a few centimetres from the body surface the plane wave approximation can be considered. Further development of this study foresees the evaluation of the pulse propagation into the human tissues considering an anatomical model of the human body and including the presence of the antenna in the case of the wearable radar system.

7. Conclusions

The interaction of UWB signals with the human body has been studied considering a plane wave incident on a layered model of the thorax. In the model, the frequency dependence of the dielectric properties of the tissues has been included.

The results show that the signal reflected from the air–skin interface can be used to detect the respiratory activity when the radar is placed at distance from the human body. On the other side, when the radar is placed close to the human body, e.g. in a breast pocket, this reflection comes at the receiving antenna superimposed to the incident signal. However, it has been shown that a small reflected signal coming from the interface between the posterior lung wall and bone could be used to detect heart and lung variations in this case.

References

Ackerman M J 1998 The visible human project *Proc. IEEE* **86** 504–11

Andrews J R 2003 UWB signal sources, antennas and propagation *Picosecond pulse labs* Application Note AN-14a

Azevedo S and McEwan T E 1996 Micropower impulse radar *Science & Technology Review* pp 17–29

Bakhtiari S, Elmer T W, Cox N M, Gopalsami N, Raptis A C, Liao S, Mikhelson I and Sahakian A V 2012 Compact millimeter-wave sensor for remote monitoring of vital signs *IEEE Trans. Instrum. Meas.* **61** 830–41

Bilich C G 2006 Bio-medical sensing using ultra wideband communications and radar technology: a feasibility study *Pervasive Health Conf. and Workshops* pp 1–9

Cavagnaro M, Pisa S and Pittella E 2013 Safety aspects of people exposed to ultra wideband radar fields *Int. J. Antennas Propag.* **2013** 7

Christ A *et al* 2010 The Virtual Family—development of surface-based anatomical models of two adults and two children for dosimetric simulations *Phys. Med. Biol.* **55** N23–38

Cole S and Cole R H 1941 Dispersion and absorption in dielectrics: I. Alternating current characteristics *J. Chem. Phys.* **9** 341–51

D'Urso M, Leone G and Soldovieri F 2009 A simple strategy for life signs detection via an X-band experimental set-up *Prog. Electromagn. Res.* C **9** 119–29

Debye P 1929 *Polar Molecules* (New York: Chemical Catalogue Company)

Dederer J, Schleicher B, De Andrade F, Tabarani S, Trasser A and Schumacher H 2007 FCC compliant 3.1–10.6 GHz UWB pulse radar system using correlation detection *Proc. IEEE/MTT-S Int. Microwave Symp. (Honolulu, 3–8 June 2007)* pp 1471–4

EC 2009 Commission of the European communities Decision 2007/131/EC April 2009

Ellis K J 1990 Reference man and woman more fully characterized *Biol. Trace Elem. Res.* **26–27** 385–400

FCC 2002 Revision of part 15 of the commission's rules regarding ultra-wideband transmission systems, FCC 02-48

Gabriel S, Lau R W and Gabriel C 1996a The dielectric properties of biological tissues: II. Measurements in the frequency range 10 Hz to 20 GHz *Phys. Med. Biol.* **41** 2251–69

Gabriel S, Lau R W and Gabriel C 1996b The dielectric properties of biological tissues: III. Parametric models for the dielectric spectrum of tissues *Phys. Med. Biol.* **41** 2271–93

ICNIRP 1998 ICNIRP Guidelines: 'Guidelines for limiting exposure to time-varying electric, magnetic, and electromagnetic fields (up to 300 GHz)' *Health Phys.* **74** 494–522

ICNIRP 2009 ICNIRP Statement on the 'Guidelines for limiting exposure to time-varying electric, magnetic, and electromagnetic fields (up to 300 GHz)' *Health Phys.* **97** 257–8

ICRP 1975 *Report of the Task Group on Reference Man: a report International Commission on Radiological Protection Task Group on Reference Man* (Oxford, New York: Pergamon)

Immoreev I Y, Samkov S and Tao T H 2005 Short-distance UWB radars *IEEE Aerosp. Electron. Syst. Mag.* **6** 9–14

Kim H J, Kim K H, Hong Y S and Choi J J 2007 Measurement of human heartbeat and respiration signals using phase detection radar *Rev. Sci. Instrum.* **78** 104703

McEwan T E 1994 Ultra-wideband radar motion sensor *US Patent* 5,361,070

Moten K, Durney C H and Stockham T G Jr 1989 Electromagnetic pulse propagation in dispersive planar dielectrics *Bioelectromagnetics* **10** 35–49

Pieraccini M, Luzi G, Dei D, Pieri L and Atzeni C 2008 Detection of breathing and heartbeat through snow using a microwave transceiver *IEEE Geosci. Remote Sens. Lett.* **5** 57–9

Pisa S, Bernardi P, Cavagnaro M, Pittella E and Piuzzi E 2012a A circuit model of an ultra wideband impulse radar system for breath activity monitoring *Int. J. Numer. Modelling: Electron. Netw. Devices Fields* **25** 46–63

Pisa S, Pittella E, Piuzzi E, Cavagnaro M and Bernardi P 2012b Design of a UWB radar system for remote breath activity monitoring *IEEE MTT-S Int. Microwave Symp. Digest (Montreal, Canada, 17–22 June 2012)* pp 1–3

Pittella E, Bernardi P, Cavagnaro M, Pisa S and Piuzzi E 2011 Design of UWB antennas to monitor cardiac activity *J. Appl. Comput. Electromagn. Soc. (ACES)* **26** 267–74

Serra A A, Nepa P, Manara G, Corsini G and Volakis J L 2010 A single on-body antenna as a sensor for cardiopulmonary monitoring *IEEE Antennas Wirel. Propag. Lett.* **9** 930–3

Sprager S and Zazula D 2012 Heartbeat and respiration detection from optical interferometric signals by using a multimethod approach *IEEE Trans. Biomed. Eng.* **59** 2922–9

Staderini E 2002 UWB radars in medicine *IEEE Aerosp. Electron. Syst. Mag.* **17** 13–8

Suzuki S, Matsui T, Asao T and Kotani K 2012 An investigation using high-precision CCD laser displacement sensor to measure body surface motion induced by heartbeat *J. Biomed. Sci. Eng.* **5** 672–7

Taylor J D and McEwan T E 2001 The micropower impulse radar *Ultra-Wideband Radar Technology* ed J D Taylor (Boca Raton, FL: CRC Press) pp 155–64

Varanini M, Berardi P C, Conforti F, Micalizzi M, Neglia D and Macerata A 2008 Cardiac and respiratory monitoring through non-invasive and contactless radar technique *Comput. Cardiol.* **35** 149–52

Varotto G and Staderini E M 2011 On the UWB medical radars working principles *Int. J. Ultra Wideband Commun. Syst.* **2** 83–93

Xiao Y, Lin J, Boric-Lubecke O and Lubecke V M 2006 Frequency-tuning technique for remote detection of heartbeat and respiration using low-power double-sideband transmission in the ka-band *IEEE Trans. Microw. Theory Tech.* **54** 2023–32

Zito D, Pepe D, Neri B, Zito F, De Rossi D and Lanatà A 2008 Feasibility study and design of a wearable system-on-a-chip pulse radar for contactless cardiopulmonary monitoring *Int. J. Telemed. Appl.* **2008** 1–10